Highly Conductive Metallic State and Strong Spin-Orbit Interaction in Annealed Germanane

Chen, Qihong; Liang, Lei; Potsi, Georgia; Wan, Puhua; Lu, Jianming; Giousis, Theodosis; Thomou, Eleni; Gournis, Dimitrios; Rudolf, Petra; Ye, Jianting

Published in:
Nano Letters

DOI:
10.1021/acs.nanolett.8b04207

NANO LETTERS

Letter

Cite This: Nano Lett. 2019, 19, 1520−1526

pubs.acs.org/NanoLett

Highly Conductive Metallic State and Strong Spin−Orbit Interaction in Annealed Germanane

Qihong Chen,[†] Lei Liang,[†] Georgia Potsi,[‡] Puhua Wan,[†] Jianming Lu,[†,§] Theodosis Giousis,[‡,∥] Eleni Thomou,[‡,∥] Dimitrios Gournis,[∥] Petra Rudolf,[‡] and Jianting Ye*[,†]

[†]Device Physics of Complex Materials, Zernike Institute for Advanced Materials, University of Groningen, Nijenborgh 4, 9747 AG Groningen, The Netherlands

[‡]Surfaces and Thin Films, Zernike Institute for Advanced Materials, University of Groningen, Nijenborgh 4, 9747 AG Groningen, The Netherlands

[§]State Key Laboratory for Mesoscopic Physics, Department of Physics, Peking University, No. 5 Yiheyuan Road Haidian District, 100871 Beijing, P. R. China

[∥]Department of Materials Science & Engineering, University of Ioannina, 45110 Ioannina, Greece

Supporting Information

ABSTRACT: Similar to carbon, germanium exists in various structures such as three-dimensional crystalline germanium and germanene, a two-dimensional germanium atomic layer. Regarding the electronic properties, they are either semiconductors or Dirac semimetals. Here, we report a highly conductive metallic state in thermally annealed germanane (hydrogen-terminated germanene, GeH), which shows a resistivity of ∼10^{-7} Ω·m that is orders of magnitude lower than any other allotrope of germanium. By comparing the resistivity, Raman spectra, and thickness change measured by AFM, we suggest the highly conductive metallic state is associated with the dehydrogenation during heating, which likely transforms germanane thin flakes to multilayer germanene. In addition, weak antilocalization is observed, serving as solid evidence for strong spin−orbit interaction (SOI) in germanane/germanene. Our study opens a possible new route to investigate the electrical transport properties of germanane/germanene, and the large SOI might provide the essential ingredients to access their topological states predicted theoretically.

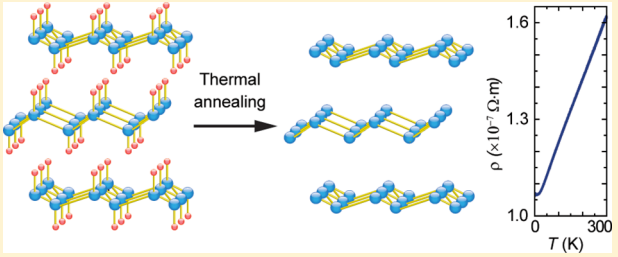

KEYWORDS: *Germanane, multilayer germanene, dehydrogenation, metallic state, weak antilocalization, strong spin−orbit interaction*

Atomically thin two-dimensional (2D) materials such as graphene,[1,2] phosphorene,[3] transition metal dichalcogenides,[4−11] etc., are regarded as promising candidates to replace conventional silicon in the next generation nanoelectronics.[12−16] Among them, 2D monolayers composed of group IV elements such as silicene[17−23] and germanene[24−28] are of particular interest because they are fully compatible with the well-established protocols for device fabrication and integration in the present silicon- and germanium-based semiconductor technologies. Similar to graphene, monolayer silicon and germanium, i.e., silicene and germanene, are both Dirac semimetals, whose band structure exhibits crossings at the K/K' points of the Brillouin zone with zero energy gap. This hallmark Dirac band structure is the origin of massless carriers, making graphene the most studied material in recent years. However, the gapless electronic structure is not favorable for making a transistor, therefore limiting the application of these Dirac materials in real devices. Compared with very stable graphene, silicene and germanene are not stable in air, which is another drawback for device applications.

Recently, hydrogen termination on graphene has been proved to be an effective way to open a band gap.[29,30] Similarly, germanane (i.e., hydrogen-terminated germanene, GeH) was synthesized by adding covalently bonded hydrogen on both sides of germanene.[31] Since the p_z orbitals of Ge bond covalently to the H atoms, the contribution of the p_z orbitals to electron transport is significantly suppressed and a direct band gap opens at the Γ points of the Brillouin zone.[32−38] As a result, a conduction band derived from the s-orbitals and a valence band derived from the p_x and p_y orbitals near the Γ point determine the transport properties. A high electron mobility is expected owing to the low effective mass.[31] The large band gap, high mobility, and low dimensionality make germanane very attractive for short-channel field effect transistors (FETs). Furthermore, the σ bond (composed of p_x and p_y orbitals) that dominates the electron transport has a

Received: October 18, 2018
Revised: January 5, 2019
Published: January 24, 2019

DOI: 10.1021/acs.nanolett.8b04207
Nano Lett. 2019, 19, 1520−1526

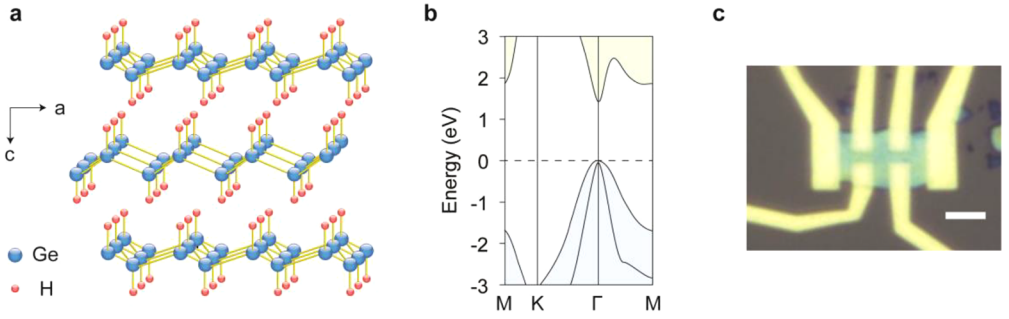

Figure 1. Germanane characteristics and device. (a) Schematic illustration of the crystal structure of germanane. Germanium atoms form a buckled honeycomb lattice in the *ab*-plane, and each germanium atom is bonded with one hydrogen atom in the *c*-direction. (b) Simplified electronic band structure of monolayer germanane. Reproduced from theoretical calculations of ref 35. (c) Optical image of a typical device on SiO_2 (300 nm)/Si (n^{++}) substrate. Scale bar: 3 μm.

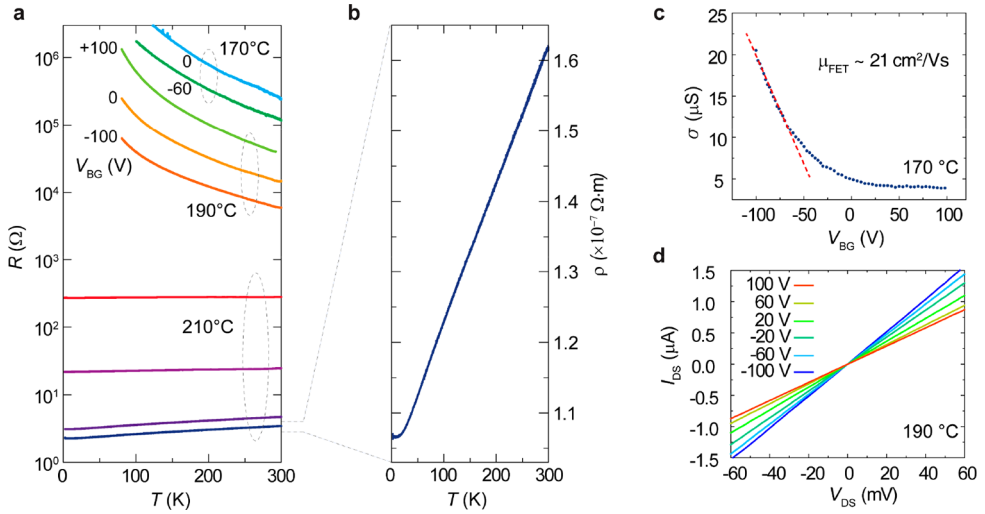

Figure 2. Insulator-to-metal transition via thermal annealing. (a) Temperature dependence of the germanane channel resistance after annealing at different temperatures, in log scale. The top two dashed circles represent results from two devices annealed at 170 and 190 °C, respectively. Different curves in each circle are measured with different back-gate voltages V_{BG} (V). The curves marked by the bottom circle are measured from three different devices after annealing at 210 °C. (b) Temperature dependence of the resistivity, corresponding to the lowest curve in (a), in linear scale. (c) Transfer curve of the device indicated by the top dashed circle in panel (a) measured at T = 300 K, showing a p-type transistor operation. The red dashed line indicates the linear fitting in the switch-on region, corresponding to a mobility of 21 $cm^2\ V^{-1}\ s^{-1}$. (d) I–V characteristics of the device indicated by the middle dashed circle in panel (a) for different back gate voltages, measured at T = 300 K.

stronger spin–orbit interaction (SOI) than the original π bond (composed of p_z orbitals); therefore, a nontrivial spin–orbit gap of ~0.2 eV opens in the valence band.[31,39] Combined with the large direct band gap, the traditional spin-selective optical process is also expected to be present in germanane, making it an attractive candidate for optoelectronic applications.

Despite the interesting properties discussed previously, very limited work has been reported regarding its electrical transport properties.[40−42] In this study, we fabricated field effect transistors based on germanane thin flakes and focused on the transport properties at low temperatures and under magnetic fields. The as-grown germanane shows very low conductivity, which agrees with the large band gap.[31,33,34] After the germanane was annealed in an inert gas atmosphere, we observe a drastic increase of the conductivity with a clear transition from insulator to metal. A p-type field effect transistor is realized on the annealed germanane. Combining the Raman spectra, AFM, and electrical transport, we suggest that the metallic behavior is likely attributed to a dehydrogenation process, which maintains the layered structure.[23] In addition, a clear weak antilocalization (WAL) feature is observed at low temperatures, indicating strong spin–orbit interaction in annealed germanane. These explorations open new opportunities for quantum and spin transport studies of germanane for both basic research and device applications.

Bulk germanane crystals were synthesized following the recently developed topotactic deintercalation method, as detailed in ref 42. In this method, $CaGe_2$ was first prepared by the reaction of high purity germanium (Ge) and calcium (Ca) in a vacuum at 950–1050 °C. Germanane was then synthesized following an exchange process between the obtained $CaGe_2$ and HCl, where Ca atoms in $CaGe_2$ are substituted by H atoms. This chemical process can be described by the equation $CaGe_2 + 2HCl \rightarrow 2GeH + CaCl_2$.

As shown in Figure 1a, a monolayer GeH has a honeycomb lattice, where each Ge is covalently bonded with another three Ge atoms in the *ab*-plane and one H atom in the *c*-direction for sp^3 hybridization. The single-crystal X-ray diffraction (XRD) shows that the unit cell is slightly distorted from the expected hexagonal lattice, becoming monoclinic with lattice parameters a = 6.924 Å, b = 3.998 Å, c = 10.939 Å, and β = 102.181°.[42] The *ab*-plane covalent bonds between Ge atoms are buckled;

DOI: 10.1021/acs.nanolett.8b04207
Nano Lett. 2019, 19, 1520−1526

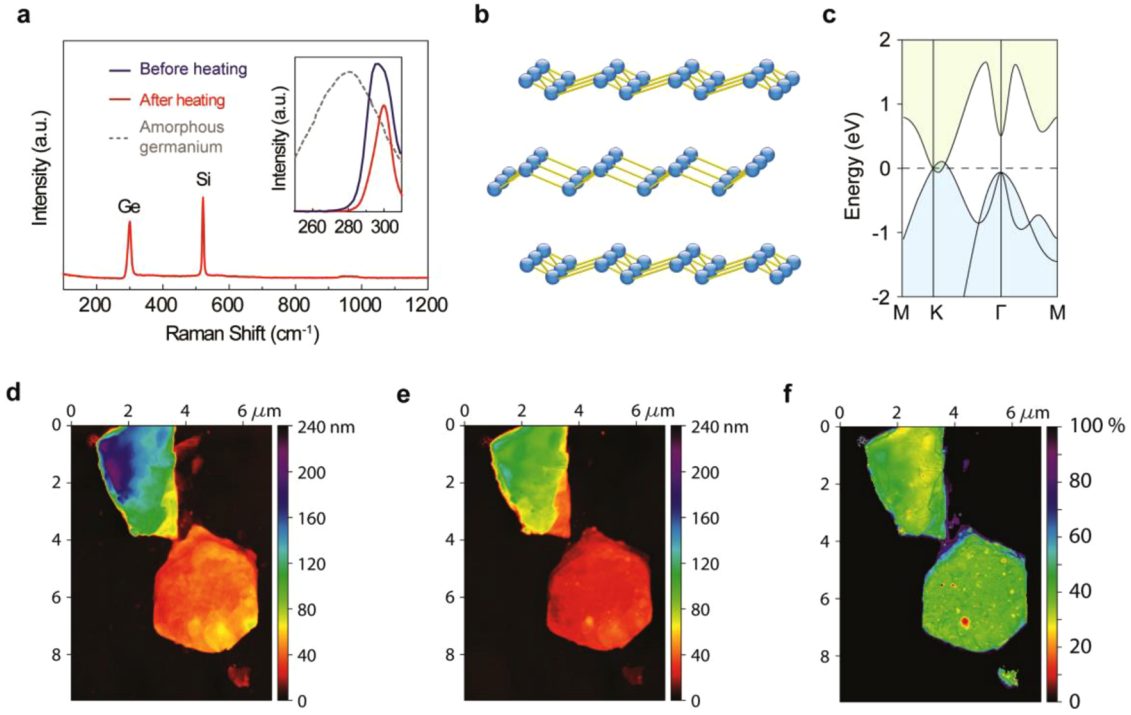

Figure 3. From germanane to germanene. (a) Raman spectra of annealed germanane. Inset: blow up of the region for the Ge−Ge vibrational mode of as-prepared germanane (dark brown), annealed germanane (red), and hydrogenated amorphous germanium (dashed gray).[44] (b) Schematic illustration of the possible crystal structure after annealing, multilayer germanene. (c) Simplified electronic band structure of bilayer germanene, with valence and conduction band crossing around *K* point. Reproduced from theoretical calculations of ref 28. (d)−(f) AFM images of germanane before annealing, after annealing at 250 °C, and the reduction of height in percentage, respectively. The spot in the top middle part with height reduction of ∼100% is the tape residue, which is completely removed after the annealing.

i.e., the two triangular sublattices are displaced relative to each other in the *c*-direction. The stacking of buckled *ab*-planes forms a layered structure with an interlayer distance of 5.5 Å. Depending on the stacking sequence, the GeH has different polytypes of 1T, 2H, and 6R.[43] The additional hydrogen bonding in the *c*-direction significantly influences the electronic structure. Figure 1b shows a simplified band structure of GeH,[31,35] where a direct band gap of ∼1.6 eV presents at the Γ point of the Brillouin zone. Chemically, while germanene is highly reactive with oxygen and therefore is normally only stable in ultrahigh vacuum or inert gas atmosphere, GeH becomes stable at ambient conditions, which is important for the following study of electrical transport. Similar to other layered materials, germanane thin flakes were prepared by mechanical exfoliation of bulk crystals on highly doped Si substrate coated with 300 nm SiO_2. Optical microscope and AFM were used to select uniform and thin flakes. We chose typical GeH flakes with thicknesses of 20−50 nm for device fabrication and subsequent electrical measurements. The electrodes, composed of Ti/Au (5/65 nm), were patterned in a Hall bar geometry via the electron-beam lithography. Figure 1c shows a typical optical image of a GeH device. The low temperature measurements were performed using either a Janis liquid nitrogen system or cryostat with a base temperature of 2 K and a 12 T magnet. Resistance was measured with a constant ac current excitation using standard lock-in amplifiers (Stanford Research SR830), and the gate voltages were set by a dc source meter (Keithley 2450).

The as-prepared device is very insulating, with room temperature sheet resistance R_s well above 10 MΩ (input impedance of the lock-in amplifier). The highly resistive state is consistent with its semiconducting nature and finite band gap (Figure 1b). After the initial characterization, the device was annealed in a tube furnace with a continuous follow of Ar gas (100 sccm) at ambient pressure. The annealing temperature was linearly ramped up to the target within 1−2 h and kept for 12 h before naturally cooling down. Figure 2a summarizes the temperature dependence of resistance after annealing. The resistance reduces to below 1 MΩ right after annealing at 170 °C. The temperature dependence of the resistance (*RT*) reveals an insulating behavior, where the resistance increases with decreasing temperature. Remarkably, the sample exhibits a clear field effect after annealing. As can be seen in Figure 2c, the transfer curve shows a p-type transistor operation where the conductivity σ increases by ∼5 times at a back gate voltage of V_{BG} = −100 V. The FET mobility can be calculated from the geometric capacitance: $\mu_{FET} = \frac{1}{C_g}\frac{d\sigma}{dV_{BG}}$, where σ is the conductivity and C_g = 11 nF/cm^2 is the gate capacitance per unit area for 300 nm SiO_2. By the linear fitting of the gate dependence of conductivity, the extracted FET mobility reaches 21 cm^2 V^{-1} s^{-1} at room temperature.

When the annealing temperature is raised to 190 °C, a significant increase in the conductivity is observed, as can be seen from the three curves labeled by the middle dashed circle in Figure 2a. Figure 2d shows the corresponding *I*−*V* characteristics of the same device measured at different back gate voltages. A consistent p-type transistor behavior is observed, as the conductivity increases at negative V_{BG}. In addition, all *I*−*V* characteristics show perfectly linear dependence, suggesting ohmic contacts between electrodes and germanane flakes. Although the overall conductivity increases

DOI: 10.1021/acs.nanolett.8b04207
Nano Lett. 2019, 19, 1520−1526

significantly compared to the sample annealed at 170 °C, the *RT* dependence still shows insulating behavior.

Only after the annealing temperature is further raised to 210 °C does the resistance decrease drastically. In contrast to the previous insulating states, a typical metallic behavior is observed, where R_s decreases with the decrease of temperature (Figure 2b). This enhanced metallicity is also accompanied by the loss of tunability by the electric field, i.e. the solid state back gate cannot tune the source-drain current I_{DS} or the channel resistance. Employing the stronger ionic gating technique,[5,7,10] the I_{DS} can be slightly tuned but the effect is also very weak (see Figure S4). The annealed germanane behaves like a piece of metal.

Germanane itself is unlikely to be turned into a metallic state because of the large band gap. The highly conductive state induced by thermal treatment immediately brings to mind the metallic state predicted for germanene, which has never been measured by electrical transport. To get a better understanding of this behavior, we measured the Raman spectra before and after thermal annealing. As shown in Figure 3a, the main peak at ∼300 cm^{-1} can be assigned to the E_2 mode of Ge−Ge vibration in the *ab*-plane.[31] This feature is very close to the Ge−Ge stretching mode of 3D crystalline germanium at 297 cm^{-1}, suggesting that attaching light H atoms has little influence on the vibration of Ge−Ge. After heating, the peak line width reduces from a fwhm (full width at half-maximum) of 18 to 10 cm^{-1}. As a reference, the gray dashed line in the inset of Figure 3a shows the Ge−Ge vibrational mode of hydrogenated amorphous germanium.[44−47] In sharp contrast, the Ge−Ge mode centered around 270 cm^{-1} is very broad with a fwhm of ∼50 cm^{-1}. This comparison rules out the formation of conventional amorphous germanium after annealing. On the contrary, the even narrower peak suggests higher crystallinity compared with the pristine GeH single crystal. The identical vibrational mode also indicates that the nature of bonding in the *ab*-plane is preserved. Consequently, we expect no change in the layered structure after annealing.

From the transport measurement, we are able to calculate the resistivity of germanane after annealing. The most conductive sample shows a resistance of ∼3 Ω at room temperature, with channel dimensions of 1.6 μm (length) × 2.5 μm (width) × 30 nm (thickness). The calculated resistivity is 1.6 × 10^{-7} Ω·m. Table 1 lists the room temperature resistivity for different materials related to our analysis.

For bulk crystalline and amorphous germanium, the resistivity at room temperature is on the order of 0.1−1 Ω·m, and the temperature dependences are dominated by the semiconducting gap and variable range hopping, where resistivity increases rapidly with the decrease of temperature.[49,53−55] From the observed metallic behavior, we can safely rule out the possibility that the annealed germanane turned into conventional crystalline or amorphous germanium. A quasi-metallic behavior can be obtained in heavily doped germanium,[50,56] in which the resistivity of ∼2 × 10^{-6} Ω·m is still 1 order of magnitude higher than our annealed germanane. Therefore, reaching the present state of low resistivity would require even higher doping, which should leave spectral signatures that are easily detectable with standard elemental analysis on degenerate-doped semiconductors. However, the combined XPS and EDX analysis (see Figure S1 of the Supporting Information) shows no trace of impurity doping. Considering the sharper Raman peak after annealing, and high quality initial single crystal of GeH, the possible production of heavily doped crystalline germanium can also be excluded. In Table 1, we can see that the resistivity of annealed germanane is even lower than graphite, and only higher than monolayer graphene. Therefore, the observed significant increase in conductivity is very likely associated with the dehydrogenation of GeH.[31] The heat treatment can break the Ge−H bond, and hydrogen atoms are released from the lattice, possibly leaving behind a multilayer germanene structure, as schematically shown in Figure 3b.

Table 1. Room Temperature Resistivity for Crystalline Germanium,[48] Amorphous Germanium,[49] Heavily Doped Germanium,[50] Graphite,[51] Annealed Germanane, and Graphene[52]

material	resistively (Ω·m)
germanium (crystalline)	0.1
germanium (amorphous)	1
germanium (heavily doped)	2 × 10^{-6}
graphite	6 × 10^{-6}
annealed GeH	1.6 × 10^{-7}
graphene	1 × 10^{-8}

As aforementioned, the two triangular sublattices of germanene are slightly displaced with respect to each other in the *c*-direction. The buckling parameter Δ, i.e., the separation between the two sublattices in the *c*-direction, is determined by the competition between the electronic and elastic energies. For free-standing monolayer germanene, the Δ calculated by density functional theory (DFT) is ∼0.65 Å.[57] With this buckling, gemanene is a 2D Dirac semimetal whose band structure exhibits a crossing at the *K*/*K*′ points with a zero density of states. Although energetically unfavorable, the Fermi levels of weakly buckled (Δ < 0.5 Å) and highly buckled monolayer germanene (Δ > 0.7−0.8 Å) cross bands below the *K*/*K*′ points with finite density of states. In annealed multilayer germanene, it is possible that the buckling of germanene deviates from the ideal free-standing value due to the interlayer interaction as well as the interaction with the underlying substrate, hence inducing metallic state with higher density of states. Consistently, calculations show that a free-standing bilayer germanene has a nonzero density of states at the Fermi level (Figure 3c).[28] This simple trend has been observed when graphene is stacked to form graphite. Similarly, a high density of states at the Fermi level is expected for multilayer germanene; hence, high electrical conductivity is expected.

It should be mentioned that dehydrogenation is also observed in a previous study[31] and the temperature lies between 200 and 250 °C, which is higher than our observation of 170−210 °C. In our experiments, we observed a strong thickness dependence of the annealing temperature necessary to induce the insulator−metal transition; i.e., following the identical procedure, thicker flakes require a higher temperature to reach the metallic state. Therefore, it is consistent that the previous dehydrogenation of bulk crystals required higher temperature. In the present study, the heating temperatures shown in Figure 2a refer to flakes that are around 30−50 nm thick.

This dehydrogenation scenario is further supported by our AFM study, as shown in Figures 3d−f. In multilayer germanane, the layers are bonded by the weak van der Waals forces, with an interlayer distance of 5.5 Å. The interlayer interaction is of comparable strength to the intralayer

DOI: 10.1021/acs.nanolett.8b04207
Nano Lett. 2019, 19, 1520−1526

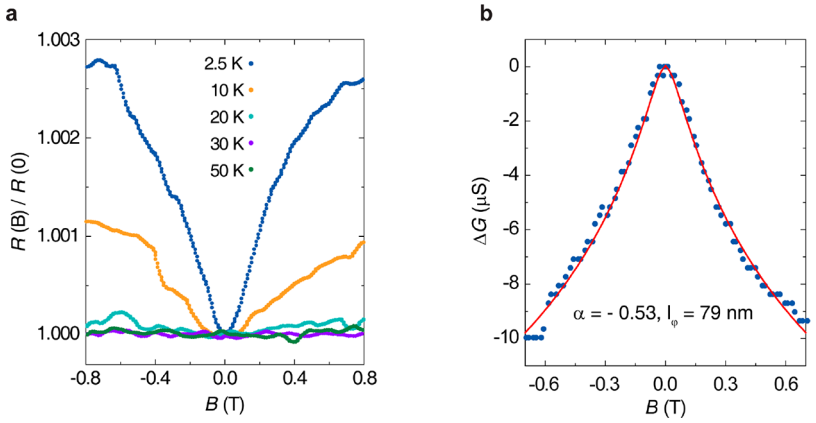

Figure 4. Evidence for strong spin−orbit interaction. (a) Normalized magnetoresistance of an annealed germanane device at different temperatures, showing clear weak antilocalization (WAL) characteristics at low field region. (b) Measured magnetoconductance (dots), which is defined as $\Delta G = G(B) - G(0)$ at $T = 2.5$ K. The red solid line is the best fitting to ΔG using the WAL equation (1), with $\alpha = -0.53$ and phase coherence length $l_\Phi = 79$ nm.

interactions, which is rather strong.[28] Consequently, the interlayer distance of germanene is much smaller than that of germanane. This has been confirmed previously by STM studies that show large flat terraces with steps of about 3.2 Å in few-layer germanene flakes grown on a gold template[26] and on an MoS_2 subtrate.[27] Comparing the AFM height profile before (Figure 3d) and after (Figure 3e) annealing at 250 °C, we observed a significant decrease in thickness. Here, we chose thicker flakes and higher annealing temperature (250 °C instead of 210 °C used in Figure 2a) for complete removal of hydrogen. Figure 3f shows a 2D map of the reduction of thickness in percentage. In spite of very different initial thicknesses in different locations, a uniform reduction of ∼40% in thickness was observed over the entire flake. Considering the change of interlayer distance, 5.5−3.2 Å/5.5 Å ≈ 42%, the observed uniform reduction of ∼40% is highly consistent with the difference of interlayer distance between germanane and germanene. Therefore, this direct measurement strongly supports the dehydrogenation process; i.e., the removal of hydrogen atoms likely transforms the multilayer system from germanane to germanene, which is consistent with the drastic enhancement of conductivity and the insulator-to-metal transition.

In addition to the metallic state of multilayer germanene discussed above, theory also predicts a strong SOI for both germanene and germanane,[32,58,59] which not only sets a good reference to further justify the aforementioned scenario but also makes multilayer germanene an attractive candidate for applications in spin-selective electronics. We measured the magnetoresistance (MR) with magnetic fields applied perpendicular to the *ab*-plane of germanane. As shown in Figure 4a, clear WAL is observed, manifesting as a characteristic sharp MR dip at $B = 0$ T. According to the 2D localization theory,[60−62] by assuming that the elastic and spin−orbit scattering times are much shorter than the inelastic scattering time, the magnetoconductivity (MC) can be described by the following equation:

$$\Delta\sigma_{2D} = \sigma_{2D}(B) - \sigma_{2D}(0) = -\frac{\alpha e^2}{2\pi^2\hbar}\left[\ln\frac{\hbar}{4Bel_\Phi^2} - \psi\left(\frac{1}{2} + \frac{\hbar}{4Bel_\Phi^2}\right)\right] \quad (1)$$

where $\hbar$ is the reduced Planck constant, e the charge of electron, $\psi(x)$ the digamma function, and l_Φ the phase coherence length. α is a fitting parameter equal to +1, 0, and −1/2 for the orthogonal, unitary, and symplectic cases, respectively.[60,63] The $\Delta\sigma_{2D}$ measured at $T = 2.5$ K is plotted in Figure 4b, where the solid curve represents the fitting with the above equation. We can see that the fitting matches very well with the experimental observation using parameters $\alpha = -0.53$ and $l_\Phi = 79$ nm. The clear WAL features provide strong evidence for strong SOI in annealed germanane.

It should be noted that the thermal property study of germanane in the previous report (Bianco et al. *ACS Nano* **2013**, *7*, 4414) also shows consistent observations with our study. In the diffuse reflectance absorption (DRA) spectroscopy, a significant red shift of the onset of optical absorption was observed after annealing, and the onset eventually decreased below that of bulk germanium. This result directly reveals the shrinking of semiconducting gap after annealing, which causes the enhancement of the electrical conductivity. Furthermore, in X-ray diffraction pattern, the 2θ value of the [002] reflection increased after annealing, directly implying a decrease of the interlayer distance along the *c*-axis.

To summarize, we measured the transport properties of annealed multilayer germanane, which has a layered structure similar to hydrogen-terminated graphene. Pristine germanane is insulating due to the finite gap in the band structure. We find that the conductivity can be gradually enhanced by thermal annealing in an Ar atmosphere, and a p-type field effect transistor is realized. After high temperature annealing, germanane becomes highly conductive and the temperature dependence of the resistance shows a metallic behavior. With a resistivity of 1.6×10^{-7} Ω·m at room temperature, a sharp Ge−Ge vibrational mode at 300 cm^{-1} in the Raman spectra, and a uniform thickness decrease of ∼40%, we suggest the product after annealing is most likely multilayer germanene, which has a structure similar to graphite. Clear weak antilocalization is observed at low temperatures with a phase coherence length of ∼80 nm, providing strong evidence for strong SOI in annealed germanane. Realizing metallic transport with strong SOI paves the way for developing field effect transistors and spin- and optoelectronic devices based on annealed germanane.

DOI: 10.1021/acs.nanolett.8b04207
Nano Lett. 2019, 19, 1520−1526

■ ASSOCIATED CONTENT

Supporting Information

The Supporting Information is available free of charge on the ACS Publications website at DOI: 10.1021/acs.nanolett.8b04207.

Elemental analysis of germanane (using XPS, EDX, and SEM), annealing temperature dependence of conductivity from the same device, field effect tuning of the intermediate dehydrogenation state, transfer curve of annealed germanane in metallic state, and Hall measurement, carrier density, and mobility of germanane in metallic state (PDF)

■ AUTHOR INFORMATION

Corresponding Author

*E-mail: j.ye@rug.nl.

ORCID

Qihong Chen: 0000-0002-6039-0456

Petra Rudolf: 0000-0002-4418-1769

Notes

The authors declare no competing financial interest.

■ ACKNOWLEDGMENTS

We thank J. Harkema, A. Joshua, and J. Zoestbergen for technical support. Q. Chen thanks the scholarship from The Ubbo Emmius Fund. J. Ye and Q. Chen thank the Stichting voor Fundamenteel Onderzoek der Materie (FOM, FV157) and FlagERA iSpinText for financial support. J. Ye acknowledges funding from the European Research Council (consolidator Grant No. 648855, Ig-QPD).

■ REFERENCES

(1) Novoselov, K. S.; Geim, A. K.; Morozov, S. V.; Jiang, D.; Zhang, Y.; Dubonos, S. V.; Grigorieva, I. V.; Firsov, A. A. Electric Field Effect in Atomically Thin Carbon Films. *Science* **2004**, *306* (5696), 666−669.

(2) Novoselov, K. S.; Jiang, D.; Schedin, F.; Booth, T. J.; Khotkevich, V. V.; Morozov, S. V.; Geim, A. K. Two-Dimensional Atomic Crystals. *Proc. Natl. Acad. Sci. U. S. A.* **2005**, *102* (30), 10451−10453.

(3) Liu, H.; Neal, A. T.; Zhu, Z.; Luo, Z.; Xu, X.; Tománek, D.; Ye, P. D. Phosphorene: An Unexplored 2D Semiconductor with a High Hole Mobility. *ACS Nano* **2014**, *8* (4), 4033−4041.

(4) Mak, K. F.; Lee, C.; Hone, J.; Shan, J.; Heinz, T. F. Atomically Thin MoS_2: A New Direct-Gap Semiconductor. *Phys. Rev. Lett.* **2010**, *105* (13), 136805.

(5) Ye, J. T.; Zhang, Y. J.; Akashi, R.; Bahramy, M. S.; Arita, R.; Iwasa, Y. Superconducting Dome in a Gate-Tuned Band Insulator. *Science* **2012**, *338* (6111), 1193−1196.

(6) Wang, Q. H.; Kalantar-Zadeh, K.; Kis, A.; Coleman, J. N.; Strano, M. S. Electronics and Optoelectronics of Two-Dimensional Transition Metal Dichalcogenides. *Nat. Nanotechnol.* **2012**, *7* (11), 699−712.

(7) Lu, J. M.; Zheliuk, O.; Leermakers, I.; Yuan, N. F. Q.; Zeitler, U.; Law, K. T.; Ye, J. T. Evidence for Two-Dimensional Ising Superconductivity in Gated MoS2. *Science* **2015**, *350* (6266), 1353−1357.

(8) Chen, Q.; Liang, L.; Ali El Yumin, A.; Lu, J.; Zheliuk, O.; Ye, J. High Quality Superconductor−Normal Metal Junction Made on the Surface of MoS_2 Flakes. *Phys. Status Solidi B* **2017**, *254*, 1700181.

(9) Shi, W.; Ye, J.; Zhang, Y.; Suzuki, R.; Yoshida, M.; Miyazaki, J.; Inoue, N.; Saito, Y.; Iwasa, Y. Superconductivity Series in Transition Metal Dichalcogenides by Ionic Gating. *Sci. Rep.* **2015**, *5*, 12534.

(10) Chen, Q. H.; Lu, J. M.; Liang, L.; Zheliuk, O.; Ali, A.; Sheng, P.; Ye, J. T. Inducing and Manipulating Heteroelectronic States in a Single MoS_2 Thin Flake. *Phys. Rev. Lett.* **2017**, *119* (14), 147002.

(11) Chen, Q.; Lu, J.; Liang, L.; Zheliuk, O.; Ali El Yumin, A.; Ye, J. Continuous Low-Bias Switching of Superconductivity in a MoS_2 Transistor. *Adv. Mater.* **2018**, *30* (28), 1800399.

(12) Zhang, W. E.; Wang, F.-C.; Yang, C. H.; Yang, M. J. The Ultimate Scaling Limit of Semiconductor-Based Transistors. *Superlattices Microstruct.* **1997**, *22* (3), 417−420.

(13) Kawaura, H.; Sakamoto, T.; Baba, T. Observation of Source-to-Drain Direct Tunneling Current in 8 Nm Gate Electrically Variable Shallow Junction Metal−Oxide−Semiconductor Field-Effect Transistors. *Appl. Phys. Lett.* **2000**, *76* (25), 3810−3812.

(14) Lundstrom, M. Moore's Law Forever? *Science* **2003**, *299* (5604), 210−211.

(15) Keyes, R. W. Physical Limits of Silicon Transistors and Circuits. *Rep. Prog. Phys.* **2005**, *68* (12), 2701.

(16) Desai, S. B.; Madhvapathy, S. R.; Sachid, A. B.; Llinas, J. P.; Wang, Q.; Ahn, G. H.; Pitner, G.; Kim, M. J.; Bokor, J.; Hu, C.; Wong, H.-S. P.; Javey, A. MoS_2 Transistors with 1-Nanometer Gate Lengths. *Science* **2016**, *354* (6308), 99−102.

(17) Aufray, B.; Kara, A.; Vizzini, S.; Oughaddou, H.; Léandri, C.; Ealet, B.; Le Lay, G. Graphene-like Silicon Nanoribbons on Ag(110): A Possible Formation of Silicene. *Appl. Phys. Lett.* **2010**, *96* (18), 183102.

(18) Lalmi, B.; Oughaddou, H.; Enriquez, H.; Kara, A.; Vizzini, S.; Ealet, B.; Aufray, B. Epitaxial Growth of a Silicene Sheet. *Appl. Phys. Lett.* **2010**, *97* (22), 223109.

(19) Tao, L.; Cinquanta, E.; Chiappe, D.; Grazianetti, C.; Fanciulli, M.; Dubey, M.; Molle, A.; Akinwande, D. Silicene Field-Effect Transistors Operating at Room Temperature. *Nat. Nanotechnol.* **2015**, *10* (3), 227−231.

(20) Chen, L.; Liu, C.-C.; Feng, B.; He, X.; Cheng, P.; Ding, Z.; Meng, S.; Yao, Y.; Wu, K. Evidence for Dirac Fermions in a Honeycomb Lattice Based on Silicon. *Phys. Rev. Lett.* **2012**, *109* (5), 056804.

(21) Vogt, P.; De Padova, P.; Quaresima, C.; Avila, J.; Frantzeskakis, E.; Asensio, M. C.; Resta, A.; Ealet, B.; Le Lay, G. Silicene: Compelling Experimental Evidence for Graphenelike Two-Dimensional Silicon. *Phys. Rev. Lett.* **2012**, *108* (15), 155501.

(22) Guzmán-Verri, G. G.; Lew Yan Voon, L. C. Electronic Structure of Silicon-Based Nanostructures. *Phys. Rev. B: Condens. Matter Mater. Phys.* **2007**, *76* (7), 075131.

(23) Lebègue, S.; Eriksson, O. Electronic Structure of Two-Dimensional Crystals from *ab Initio* Theory. *Phys. Rev. B: Condens. Matter Mater. Phys.* **2009**, *79* (11), 115409.

(24) Ni, Z.; Liu, Q.; Tang, K.; Zheng, J.; Zhou, J.; Qin, R.; Gao, Z.; Yu, D.; Lu, J. Tunable Bandgap in Silicene and Germanene. *Nano Lett.* **2012**, *12* (1), 113−118.

(25) Dávila, M. E.; Xian, L.; Cahangirov, S.; Rubio, A.; Le Lay, G. Germanene: A Novel Two-Dimensional Germanium Allotrope Akin to Graphene and Silicene. *New J. Phys.* **2014**, *16* (9), 095002.

(26) Dávila, M. E.; Le Lay, G. Few Layer Epitaxial Germanene: A Novel Two-Dimensional Dirac. *Sci. Rep.* **2016**, *6*, 20714.

(27) Zhang, L.; Bampoulis, P.; Rudenko, A. N.; Yao, Q.; van Houselt, A.; Poelsema, B.; Katsnelson, M. I.; Zandvliet, H. J. W. Structural and Electronic Properties of Germanene on MoS_2. *Phys. Rev. Lett.* **2016**, *116* (25), 256804.

(28) Acun, A.; Zhang, L.; Bampoulis, P.; Farmanbar, M.; vanHouselt, A.; Rudenko, A. N.; Lingenfelder, M.; Brocks, G.; Poelsema, B.; Katsnelson, M. I.; Zandvliet, H. J. W. Germanene: The Germanium Analogue of Graphene. *J. Phys.: Condens. Matter* **2015**, *27* (44), 443002.

(29) Elias, D. C.; Nair, R. R.; Mohiuddin, T. M. G.; Morozov, S. V.; Blake, P.; Halsall, M. P.; Ferrari, A. C.; Boukhvalov, D. W.; Katsnelson, M. I.; Geim, A. K.; Novoselov, K. S. Control of Graphene's Properties by Reversible Hydrogenation: Evidence for Graphane. *Science* **2009**, *323* (5914), 610−613.

DOI: 10.1021/acs.nanolett.8b04207
Nano Lett. 2019, 19, 1520−1526

(30) Sofo, J. O.; Chaudhari, A. S.; Barber, G. D. Graphane: A Two-Dimensional Hydrocarbon. *Phys. Rev. B: Condens. Matter Mater. Phys.* **2007**, *75* (15), 153401.
(31) Bianco, E.; Butler, S.; Jiang, S.; Restrepo, O. D.; Windl, W.; Goldberger, J. E. Stability and Exfoliation of Germanane: A Germanium Graphane Analogue. *ACS Nano* **2013**, *7* (5), 4414−4421.
(32) Amamou, W.; Odenthal, P. M.; Bushong, E. J.; O'Hara, D. J.; Luo, Y. K.; van Baren, J.; Pinchuk, I.; Wu, Y.; Ahmed, A. S.; Katoch, J.; Bockrath, M. W.; Tom, H. W. K.; Goldberger, J. E.; Kawakami, R. K. Large Area Epitaxial Germanane for Electronic Devices. *2D Mater.* **2015**, *2* (3), 035012.
(33) Luo, X.; Zurek, E. Crystal Structures and Electronic Properties of Single-Layer, Few-Layer, and Multilayer GeH. *J. Phys. Chem. C* **2016**, *120* (1), 793−800.
(34) Voon, L. C. L. Y.; Sandberg, E.; Aga, R. S.; Farajian, A. A. Hydrogen Compounds of Group-IV Nanosheets. *Appl. Phys. Lett.* **2010**, *97* (16), 163114.
(35) Houssa, M.; Scalise, E.; Sankaran, K.; Pourtois, G.; Afanas'ev, V. V.; Stesmans, A. Electronic Properties of Hydrogenated Silicene and Germanene. *Appl. Phys. Lett.* **2011**, *98* (22), 223107.
(36) Lebègue, S.; Klintenberg, M.; Eriksson, O.; Katsnelson, M. I. Accurate Electronic Band Gap of Pure and Functionalized Graphane from GW Calculations. *Phys. Rev. B: Condens. Matter Mater. Phys.* **2009**, *79* (24), 245117.
(37) Zhao, Y.; Yin, D.; Yoon, Y. Intrinsic Performance of Germanane Schottky Barrier Field-Effect Transistors. *IEEE Trans. Electron Devices* **2018**, *65*, 4188−4195.
(38) Yao, Q.; Zhang, L.; Kabanov, N. S.; Rudenko, A. N.; Arjmand, T.; Rahimpour Soleimani, H.; Klavsyuk, A. L.; Zandvliet, H. J. W. Bandgap Opening in Hydrogenated Germanene. *Appl. Phys. Lett.* **2018**, *112* (17), 171607.
(39) Liu, C.-C.; Feng, W.; Yao, Y. Quantum Spin Hall Effect in Silicene and Two-Dimensional Germanium. *Phys. Rev. Lett.* **2011**, *107* (7), 076802.
(40) Sahoo, N. G.; Esteves, R. J.; Punetha, V. D.; Pestov, D.; Arachchige, I. U.; McLeskey, J. T., Jr. Schottky Diodes from 2D Germanane. *Appl. Phys. Lett.* **2016**, *109* (2), 023507.
(41) Young, J. R.; Chitara, B.; Cultrara, N. D.; Arguilla, M. Q.; Jiang, S.; Fan, F.; Johnston-Halperin, E.; Goldberger, J. E. Water Activated Doping and Transport in Multilayered Germanane Crystals. *J. Phys.: Condens. Matter* **2016**, *28* (3), 034001.
(42) Madhushankar, B. N.; Kaverzin, A.; Giousis, T.; Potsi, G.; Gournis, D.; Rudolf, P.; Blake, G. R.; van der Wal, C. H.; van Wees, B. J. Electronic Properties of Germanane Field-Effect Transistors. *2D Mater.* **2017**, *4* (2), 021009.
(43) Cultrara, N. D.; Wang, Y.; Arguilla, M. Q.; Scudder, M. R.; Jiang, S.; Windl, W.; Bobev, S.; Goldberger, J. E. Synthesis of 1T, 2H, and 6R Germanane Polytypes. *Chem. Mater.* **2018**, *30* (4), 1335−1343.
(44) Chaudhuri, S.; Shen, L.; Healy, N.; Peacock, A. C.; Badding, J. V. *Hydrogenated Amorphous Germanium Optical Fiber. Novel Optical Materials and Applications*; Optical Society of America, 2015; NT2C.4.
(45) Wihl, M.; Cardona, M.; Tauc, J. Raman Scattering in Amorphous Ge and III−V Compounds. *J. Non-Cryst. Solids* **1972**, *8*, 172−178.
(46) Bermejo, D.; Cardona, M. Raman Scattering in Pure and Hydrogenated Amorphous Germanium and Silicon. *J. Non-Cryst. Solids* **1979**, *32* (1), 405−419.
(47) Veldhuizen, L. W.; van der Werf, C. H. M.; Kuang, Y.; Bakker, N. J.; Yun, S. J.; Schropp, R. E. I. Optimization of Hydrogenated Amorphous Silicon Germanium Thin Films and Solar Cells Deposited by Hot Wire Chemical Vapor Deposition. *Thin Solid Films* **2015**, *595*, 226−230.
(48) Hung, C. S.; Gliessman, J. R. Resistivity and Hall Effect of Germanium at Low Temperatures. *Phys. Rev.* **1954**, *96* (5), 1226−1236.
(49) Clark, A. H. Electrical and Optical Properties of Amorphous Germanium. *Phys. Rev.* **1967**, *154* (3), 750−757.
(50) Trumbore, F. A.; Tartaglia, A. A. Resistivities and Hole Mobilities in Very Heavily Doped Germanium. *J. Appl. Phys.* **1958**, *29* (10), 1511−1511.
(51) Tyler, W. W.; Wilson, A. C. Thermal Conductivity, Electrical Resistivity, and Thermoelectric Power of Graphite. *Phys. Rev.* **1953**, *89* (4), 870−875.
(52) Chen, J.-H.; Jang, C.; Xiao, S.; Ishigami, M.; Fuhrer, M. S. Intrinsic and Extrinsic Performance Limits of Graphene Devices on SiO_2. *Nat. Nanotechnol.* **2008**, *3* (4), 206−209.
(53) Sharma, S. K.; Jain, S. C.; Aggarwal, S. S.; Bhide, V. G. Structure and Electrical Resistivity of Thin Amorphous Germanium Films. *J. Non-Cryst. Solids* **1972**, *7* (3), 285−294.
(54) Pollak, M.; Knotek, M. L.; Kurtzman, H.; Glick, H. Dc Conductivity of Amorphous Germanium and the Structure of the Pseudogap. *Phys. Rev. Lett.* **1973**, *30* (18), 856−859.
(55) Čápek, V.; Koc, S.; Zemek, J. DC Conductivity of Amorphous Germanium. *J. Non-Cryst. Solids* **1975**, *18* (1), 95−106.
(56) Thieme, W.; Diletti, H.; Coufal, H.; Gierisch, W.; Lüscher, E. The Electrical Resistivity of Highly Doped P-Type Germanium from 40 mK to 300 K. *J. Less-Common Met.* **1978**, *62*, 405−406.
(57) Cahangirov, S.; Topsakal, M.; Aktürk, E.; Şahin, H.; Ciraci, S. Two- and One-Dimensional Honeycomb Structures of Silicon and Germanium. *Phys. Rev. Lett.* **2009**, *102* (23), 236804.
(58) Seixas, L.; Padilha, J. E.; Fazzio, A. Quantum Spin Hall Effect on Germanene Nanorod Embedded in Completely Hydrogenated Germanene. *Phys. Rev. B: Condens. Matter Mater. Phys.* **2014**, *89* (19), 195403.
(59) Si, C.; Liu, J.; Xu, Y.; Wu, J.; Gu, B.-L.; Duan, W. Functionalized Germanene as a Prototype of Large-Gap Two-Dimensional Topological Insulators. *Phys. Rev. B: Condens. Matter Mater. Phys.* **2014**, *89* (11), 115429.
(60) Hikami, S.; Larkin, A. I.; Nagaoka, Y. Spin-Orbit Interaction and Magnetoresistance in the Two Dimensional Random System. *Prog. Theor. Phys.* **1980**, *63* (2), 707−710.
(61) McCann, E.; Kechedzhi, K.; Fal'ko, V. I.; Suzuura, H.; Ando, T.; Altshuler, B. L. Weak-Localization Magnetoresistance and Valley Symmetry in Graphene. *Phys. Rev. Lett.* **2006**, *97* (14), 146805.
(62) He, H.-T.; Wang, G.; Zhang, T.; Sou, I.-K.; Wong, G. K. L.; Wang, J.-N.; Lu, H.-Z.; Shen, S.-Q.; Zhang, F.-C. Impurity Effect on Weak Antilocalization in the Topological Insulator Bi_2Te_3. *Phys. Rev. Lett.* **2011**, *106* (16), 166805.
(63) Dyson, F. J. Statistical Theory of the Energy Levels of Complex Systems. I. *J. Math. Phys.* **1962**, *3* (1), 140−156.

DOI: 10.1021/acs.nanolett.8b04207
Nano Lett. 2019, 19, 1520−1526